Hybrid neutron stars in the Thomas-Fermi theory

M. Ghazanfari Mojarrad* and J. Ranjbar
Department of Physics, Faculty of Science, University of Kashan, P.O. Box 87317-51167, Kashan, Iran

(Received 14 November 2018; revised manuscript received 11 June 2019; published 22 July 2019)

The baryon-quark phase transition is studied for the equation of state (EOS) of neutron star (NS) matter. The Thomas-Fermi (TF) approximation is employed in a semiclassical mean-field (MF) model for the EOS of baryonic matter including hyperons. The EOS of quark matter is also extracted from the Nambu–Jona-Lasinio (NJL) model. The phase transition from baryons to quarks is considered in the NS structure under the Maxwell and Gibbs constructions. Our findings for the maximum mass of NSs, as compared with the almost $2M_\odot$ pulsars J1614 − 2230 and J0348 + 0432, indicate that a region of baryon-quark mixed phase can exist in the inner core of NSs, while the existence of a pure phase is not allowed.

DOI: 10.1103/PhysRevC.100.015804

I. INTRODUCTION

Neutron stars (NSs) are basic laboratories for the physics of dense matter. These compact objects can be formed at the last stage of the gravitational collapse in massive stars with $8M_\odot$–$20M_\odot$ [1–4]. It is generally understood that a thin solid crust and a thick liquid core constitute the main structure of an NS. Approaching the center of an NS, the mass (energy) density ranges from about the nuclear saturation value $e_o \simeq 2.68 \times 10^{14} \frac{\mathrm{g}}{\mathrm{cm}^3}$ (150 MeV fm^{-3}) to several times higher. Thus, the equation of state (EOS) of baryonic matter has a key role in understanding the structure and composition of NSs [5–7]. On this basis, enormous efforts have focused on the baryonic EOS for NS modeling over the last few decades. The EOS of such matter has been investigated either by microscopic models, which are based on realistic interactions extracted from nucleon-nucleon scattering data [8–11], or by phenomenological models, where the parameters of interactions are fixed to fulfill the saturation properties of normal nuclear matter [12–15]. However, it is an advantage for a model to provide the simplest possible procedure for determining the baryonic EOS. Hence, such a significant advantage can be found in the Thomas-Fermi (TF) approximation as an efficient many-body approach when used in a semiclassical mean-field (MF) model [16–23]. To this purpose, the EOS of NS matter has been investigated successfully in Refs. [14,15]. In the previous work [15], the role of β-stable strange matter in a stiff enough EOS, required for a $2M_\odot$ NS, was investigated by using generalized baryon–baryon interactions in phase space. However, a comprehensive understanding of the structure and composition of NSs is far from being achieved. It is expected that NS matter could undergo a phase transition from baryonic matter to quark matter in the interior of NSs [24–39]. In general, the existence of hyperon and quark degrees of freedom at high baryonic densities softens the EOS and lowers the maximum mass of NSs. Therefore, since the recent observations of $2M_\odot$ pulsars [40–42] have imposed a severe constraint on the maximum mass of NSs, investigating the baryon-quark phase transition is considered to be a challenging issue in astrophysics.

In this research, the baryon-quark phase transition in NS matter is studied by using the TF model for baryonic matter and the Nambu–Jona-Lasinio (NJL) model [43,44] for quark matter. Based on this idea, the paper is organized as follows. In Sec. II, the formalism for the EOS of baryonic and quark matter is presented on the basis of the TF and NJL models, respectively. Furthermore, the Maxwell and Gibbs constructions are illustrated for the baryon-quark phase transition. Section III is devoted to the discussion about the results obtained for the baryon-quark phase transition in NS matter, and finally, the summary and conclusions are given in Sec. IV.

II. FORMALISM

The baryonic EOS of NS matter is described in the TF approximation by using a semiclassical MF model. In a semiclassical approach, the state of each particle is specified by its momentum and position in phase space. This approximation is suitable when the MF potential has a smooth behavior [45]. In this section, the EOS of quark matter is also described by the NJL model. Furthermore, our attention is paid to the baryon-quark phase transition under the Maxwell and Gibbs constructions.

A. TF model for baryonic matter

Based on the Myers and Swiatecki (MS) interactions [16,17], the generalized interactions GTF(90) and GTF(96) [15] are used for the EOS of baryonic matter in which baryons are in β equilibrium with relativistic electrons and muons. Within these generalized Yukawa interactions, the

*Corresponding author: ghazanfari@kashanu.ac.ir

baryon-baryon interactions are given as follows [15]:

$$V_{12} = -2\, G_{B1,B2}\, \rho_0^{-1} f\left(\frac{r_{12}}{a}\right) \left\{ \frac{1}{2}(1 \mp \xi)\alpha - \frac{1}{2}(1 \mp \zeta)\left[\bar{\chi}\beta \left(\frac{p_{12}}{p_b}\right)^2 - \gamma \left(\frac{p_b}{|p_{12}|}\right) + \bar{\chi}\sigma \left(\frac{2\bar{\rho}}{\rho_0}\right)^{\frac{2}{3}} \right] \right\}, \tag{1}$$

with

$$f\left(\frac{r_{12}}{a}\right) = \frac{1}{4\pi a^3} \frac{\exp\left(-\frac{r_{12}}{a}\right)}{\frac{r_{12}}{a}}, \quad \bar{\rho}^{\frac{2}{3}} = \frac{1}{2}\left(\rho_1^{\frac{2}{3}} + \rho_2^{\frac{2}{3}}\right). \tag{2}$$

Here, $r_{12} = |\vec{r}_1 - \vec{r}_2|$ and $p_{12} = |\vec{p}_1 - \vec{p}_2|$ are the position and relative momentum for each pair of baryons in phase space, respectively. The mean density $\bar{\rho}$ is also defined as a function of ρ_1 and ρ_2, which are the densities of each pair of baryons at the positions $\vec{r}_1$ and $\vec{r}_2$, respectively. Clearly, the strength of these Yukawa-type interactions depends explicitly on the momentum and density. The seven flexible parameters $(a, \xi, \zeta, \alpha, \beta, \gamma, \sigma)$ in GTF(90) [GTF(96)] are fixed to reproduce the saturation properties of normal nuclear matter as well as the coefficients of the Weizsacher-Bethe semiempirical mass formula [16,17]:

$$\begin{aligned} &a = 0.59542\ (0.59294)\ \text{fm}, \quad \alpha = 3.60928\ (1.94684),\\ &\beta = 0.37597\ (0.15311), \quad \gamma = 0.21329\ (1.13672),\\ &\sigma = 1.33677\ (1.05), \quad \xi = 0.44003\ (0.27976),\\ &\zeta = 0.59778\ (0.55665). \end{aligned} \tag{3}$$

The saturation density and Fermi momentum of normal nuclear matter are incorporated into these interactions by the coefficients $\rho_0 = (\frac{4}{3}\pi r_0^3)^{-1}$ and $p_b = \hbar(\frac{3}{2}\pi^2\rho_0)^{\frac{1}{3}}$, respectively. Here, $r_0 = 1.13$ (1.14) is the nuclear matter radius for GTF(90) [GTF(96)] and $T_b = \frac{p_b^2}{2\bar{m}} = 37.679$ (37.021) MeV is the associated kinetic energy with the average nucleonic mass $\bar{m} = 938.903\ \text{MeV}/c^2$. In order to make a distinction among the interactions between pairs of baryons, the upper sign for like and the lower sign for unlike particles are assigned. Choosing $\xi \neq \zeta$ gives an improved description of asymmetric nuclear systems especially for higher asymmetry parameters. The saturation mechanism is handled through the competition between the attractive terms having α and γ coefficients and the repulsive terms having β and σ coefficients. In general, repulsive interactions are expected to dominate the EOS at high baryonic densities. Thus, without loss of generality, the repulsive effects of β and σ coefficients are amplified by the phenomenological factor $\bar{\chi} = (\frac{\rho_B}{\rho_0})^{\frac{2}{3}}$ [15] instead of $\bar{\chi} = 1$ in the MS interactions [16,17]. Here, $G_{B1,B2}$ is the coupling constant of each baryon-baryon interaction, e.g., $G_{N,N} = T_b$ is the one for the nucleon-nucleon interaction. According to the available hypernuclear experimental data, Λ hyperon gets the best-known adjustable potential well $U_\Lambda^{(N)} \cong -30$ MeV at the saturation density of normal nuclear matter [46]. In addition, unlike the Λ-N interaction, the other hyperonic potential wells cannot be firmly estimated, since the related hypernuclear experimental data are scarce and ambiguous. By introducing $U_b^{(b')}$ as the potential felt by the bth baryon at the saturation density of type b'th baryonic matter, the following values $U_\Sigma^{(N)} \cong +30$ MeV and $U_\Xi^{(N)} \cong -18$ MeV [47] and the following relations [33,48] can be generally admitted:

$$\begin{aligned} U_\Xi^{(\Xi)} \cong U_\Sigma^{(\Xi)} \cong U_\Lambda^{(\Xi)} \cong U_\Sigma^{(\Sigma)} \cong U_\Xi^{(\Sigma)} \cong U_\Lambda^{(\Sigma)} \cong 2U_\Lambda^{(\Lambda)} \\ \cong 2U_\Xi^{(\Lambda)} \cong 2U_\Sigma^{(\Lambda)} \cong -10\ (\text{MeV}). \end{aligned} \tag{4}$$

Consequently, according to the above constraints, the coupling constants $G_{B1,B2}$ can be adjusted to the values reported in Table I.

TABLE I. Hyperon-nucleon and hyperon-hyperon coupling constants in the GTF(90) and GTF(96) interactions.

Coupling constant	GTF(90) $T_b = 37.679$ MeV	GTF(96) $T_b = 37.021$ MeV
$G_{\Lambda,N}$	$\frac{T_b}{5.25}$	$\frac{T_b}{5.14}$
$G_{\Sigma,N}$	$-\frac{T_b}{5.25}$	$-\frac{T_b}{5.14}$
$G_{\Xi,N}$	$\frac{T_b}{8.75}$	$\frac{T_b}{8.57}$
$G_{\Xi,\Xi}$, $G_{\Sigma,\Sigma}$	$\frac{T_b}{2.12}$	$\frac{T_b}{2.17}$
$G_{\Lambda,\Lambda}$, $G_{\Sigma,\Lambda}$, $G_{\Xi,\Lambda}$	$\frac{T_b}{4.24}$	$\frac{T_b}{4.35}$
$G_{\Sigma,\Xi}$, $G_{\Xi,\Sigma}$, $G_{\Lambda,\Xi}$, $G_{\Lambda,\Sigma}$	$\frac{T_b}{3.24}$	$\frac{T_b}{3.15}$

Within the TF model, the baryonic energy density can be written as

$$e_{\text{TF}} = \frac{2}{h^3} \sum_{b=n^0,p^+,\Lambda^0,\Sigma^0,\Sigma^-,\Sigma^+,\Xi^0,\Xi^-} \int d^3p_1 \times \left(m_b c^2 + \frac{p_1^2}{2m_b} + \frac{1}{2}V_b(p_1) \right) \Theta(p_{F,b} - p_1), \tag{5}$$

where $p_{F,b}$ is the Fermi momentum of bth baryon. Here, $V_b(p_1)$ as the MF potential of bth baryon can be expressed as follows:

$$V_b(p_1) = V_b^b(p_1) + \sum_{b' \neq b} V_b^{b'}(p_1), \tag{6}$$

with

$$\begin{aligned} V_b^b(p_1) &= -\frac{4}{\rho_0 h^3}\left[G_{b,b} \int_0^{p_{F,b}} d^3p_2 \left(\alpha_l - \beta_l \left(\frac{p_{12}}{p_b}\right)^2 + \gamma_l \frac{p_b}{|p_{12}|} - \sigma_l \left(\frac{2\bar{\rho}}{\rho_0}\right)^{\frac{2}{3}} \right) \right], \\ V_b^{b'}(p_1) &= -\frac{4}{\rho_0 h^3}\left[\sum_{b' \neq b} G_{b,b'} \int_0^{p_{F,b'}} d^3p_2 \left(\alpha_u - \beta_u \left(\frac{p_{12}}{p_b}\right)^2 + \gamma_u \frac{p_b}{|p_{12}|} - \sigma_u \left(\frac{2\bar{\rho}}{\rho_0}\right)^{\frac{2}{3}} \right) \right]. \end{aligned} \tag{7}$$

The interaction between like and unlike particles can be distinguished by l and u indices, where the minus and plus signs indicate the like and unlike particles, respectively:

$$\alpha_{l,u} = \tfrac{1}{2}(1 \mp \xi)\alpha,\ \beta_{l,u} = \tfrac{1}{2}(1 \mp \zeta)\bar{\chi}\beta,\ \gamma_{l,u} = \tfrac{1}{2}(1 \mp \zeta)\gamma,\quad \sigma_{l,u} = \tfrac{1}{2}(1 \mp \zeta)\bar{\chi}\sigma. \tag{8}$$

Finally, the baryonic energy density is specified by including the density of each baryon ρ_b in the following form:

$$\begin{aligned} e_{\rm TF} = &\sum_{b,(b'\neq b)} \frac{2G_{b,b}}{\rho_0}\left\{\frac{\rho_0\kappa_b}{2} - \frac{\alpha_l\rho_b^2}{2} + \beta_l\rho_b\kappa_b - \frac{64\pi^2 p_b\gamma_l p_{F,b}^5}{15h^6} + \frac{\sigma_l\rho_0}{4}\left[\left(\frac{2\rho_b}{\rho_0}\right)^{\frac{5}{3}}\rho_b\right]\right\} \\ &+\frac{2G_{b,b'}}{\rho_0}\left\{-\frac{\alpha_u\rho_b\rho_{b'}}{2} + \beta_u\rho_b\kappa_{b'} - \frac{16\pi^2 p_b\gamma_u}{h^6}\left[\left(\frac{p_{F,<}^3 p_{F,>}^2}{3} - \frac{p_{F,<}^5}{15}\right)\right] + \frac{\sigma_u\rho_0}{4}\left[\left(\frac{2\rho_b}{\rho_0}\right)^{\frac{5}{3}}\rho_{b'}\right]\right\}, \end{aligned} \tag{9}$$

with

$$p_{F,b(b')} = \left(\frac{3h^3\rho_{b(b')}}{8\pi}\right)^{\frac{1}{3}},\quad \kappa_{b(b')} = \frac{8\pi p_b^2 p_{F,b(b')}^5}{h^3}. \tag{10}$$

According to the second law of thermodynamics, the following relations between the chemical potential of baryons and leptons are imposed by the β-equilibrium conditions:

$$\mu_{p^+} = \mu_{\Sigma^+} = \mu_n - \mu_{e^-}, \tag{11}$$

$$\mu_{\Lambda^0} = \mu_{\Sigma^0} = \mu_{\Xi^0} = \mu_n, \tag{12}$$

$$\mu_{\Sigma^-} = \mu_{\Xi^-} = \mu_n + \mu_{e^-}, \tag{13}$$

$$\mu_{\mu^-} = \mu_{e^-}. \tag{14}$$

The chemical potential of bth baryon can be explicitly obtained as follows:

$$\mu_b = \frac{\partial e_{\rm TF}}{\partial\rho_b} = m_b c^2 + \frac{p_{F,b}^2}{2m_b} + \mu_b^{(l)} + \mu_b^{(u)}, \tag{15}$$

with

$$\begin{aligned} \mu_b^{(l)} &= \frac{2G_{b,b}}{\rho_0}\left\{-\alpha_l\rho_b + \beta_l\rho_b\left(\frac{p_{F,b}}{p_b}\right)^2 + \beta_l\kappa_b + \sigma_l\left(\frac{2\varrho_b}{\rho_0}\right)^{\frac{2}{3}}\rho_b - \gamma_l\left(\frac{8\pi p_b}{h^3}\right)\left(\frac{p_{F,b}^2}{3}\right)\right\}, \\ \mu_b^{(u)} &= \sum_{b'\neq b}\frac{2G_{b,b'}}{\rho_0}\left\{-\alpha_u\rho_{b'} + \beta_u\rho_{b'}\left(\frac{p_{F,b}}{p_b}\right)^2 + \beta_u\kappa_{b'} + \sigma_u\left(\frac{2\varrho_b}{\rho_0}\right)^{\frac{2}{3}}\left(\frac{5\rho_{b'}}{6}\right) + \sigma_u\left(\frac{2\varrho_{b'}}{\rho_0}\right)^{\frac{2}{3}}\left(\frac{\rho_{b'}}{2}\right)\right. \\ &\left.-\gamma_u\left(\frac{8\pi p_b}{h^3}\right)\left[\left(\frac{p_{F,b'}^3}{3p_{F,b}}\ \text{for}\ p_{F,b} \geqslant p_{F,b'}\right)\ \text{or}\ \left(\frac{p_{F,b'}^2}{2} - \frac{p_{F,b}^2}{6}\ \text{for}\ p_{F,b'} \geqslant p_{F,b}\right)\right]\right\}. \end{aligned} \tag{16}$$

In addition, the composition of baryonic matter is constrained by the charge neutrality condition:

$$y_{p^+} + y_{\Sigma^+} = y_{e^-} + y_{\mu^-} + y_{\Sigma^-} + y_{\Xi^-}. \tag{17}$$

In our notation, $y_i = \frac{\rho_i}{\rho_B}$ is introduced as the relative fraction of the ith baryon or lepton.

The chemical potential of each lepton is given by its Fermi energy:

$$\mu_{l=e^-,\mu^-} = \sqrt{(p_{F,l}\,c)^2 + (m_l c^2)^2},\qquad p_{F,l} = \left(\frac{3h^3\rho_l}{8\pi}\right)^{\frac{1}{3}}. \tag{18}$$

At a given baryonic density, the basic quantities for determination of thermodynamic properties of baryonic matter can be self-consistently calculated through Eqs. (11)–(14). The total energy density of baryonic matter can be calculated when the leptonic energy density contribution is also included:

$$e_B = e_{\rm TF} + e_L, \tag{19}$$

where

$$e_L = \frac{2}{h^3}\sum_{l=e^-,\mu^-}\int_0^{p_{F,l}} d^3p\sqrt{(pc)^2 + (mc^2)^2}. \tag{20}$$

Furthermore, through the first derivative of the baryonic energy density with respect to the total density $\rho = \sum_{k=b,l}\rho_k$, the baryonic pressure can be determined as follows:

$$P_B = \rho^2\frac{\partial(e_B/\rho)}{\partial\rho} = P_{\rm TF} + P_L = \sum_{k=b,l}(\mu_k\rho_k) - e_B. \tag{21}$$

B. NJL model for quark matter

The NJL model can successfully reproduce many aspects of quantum chromodynamics (QCD) such as the nonperturbative vacuum structure and dynamical breaking of chiral symmetry [44]. In this work, a three-flavor version of the NJL model is adopted to describe the EOS of quark matter. The QCD Lagrangian can be written as

$$\begin{aligned}\mathcal{L}_{\rm NJL} &= \bar{q}(i\gamma_\mu\partial^\mu - m^0)q + G_S\sum_{a=0}^{8}[(\bar{q}\lambda_a q)^2 + (\bar{q}\gamma_5\lambda_a q)^2] \\ &\quad -K\{\det[\bar{q}(1+\gamma_5)q] + \det[\bar{q}(1-\gamma_5)q]\} \\ &\quad -G_V\sum_{a=0}^{8}[(\bar{q}\gamma_\mu\lambda_a q)^2 + (\bar{q}\gamma_5\gamma_\mu\lambda_a q)^2], \end{aligned} \tag{22}$$

where q signifies a quark field including the contributions of three active flavors ($N_f = 3$) and three colors ($N_c = 3$). The current quark mass matrix $m^0 = \mathrm{diag}(m_u^0, m_d^0, m_s^0)$ is also included in the Lagrangian. Here, λ_a with $a = 1, 2, \ldots, 8$ are the well-known Gell-Mann matrices in the color space and $\lambda_0 = \sqrt{2/3}\,\mathbb{I}_{3\times3}$. In the present calculations, $m_u^0 = m_d^0 = 5.5\,\mathrm{MeV}$, $m_s^0 = 140.7\,\mathrm{MeV}$, and the parameters $\Lambda = 602.3\,\mathrm{MeV}$, $G_S = \frac{1.835}{\Lambda^2}$, and $K = \frac{12.36}{\Lambda^5}$ are adopted from Ref. [49]. The vector coupling constant G_V is considered as a free parameter, due to the uncertainty in the theoretical predictions of the ratio G_V/G_S [50]. However, the value of this ratio is expected to lie in the range 0–0.5 [51].

Within the MF approximation under conditions where $G_V = 0$, the dynamically generated quark mass M_i and the quark chemical potential μ_i are obtained by solving the gap equation as follows [33]:

$$M_i = m_i^0 - 4G_S\langle\bar{q}_i q_i\rangle + 2K\langle\bar{q}_j q_j\rangle\langle\bar{q}_k q_k\rangle, \tag{23}$$

$$\mu_i = \sqrt{\left(p_F^i\right)^2 + (M_i)^2}. \tag{24}$$

In Eq. (23), (i, j, k) indicate any permutation of (u, d, s) quarks. The scaler condensate $C_i = \langle\bar{q}_i q_i\rangle$ is given by

$$C_i = -\frac{3}{\pi^2}\int_{p_F^i}^{\Lambda}\frac{M_i}{\sqrt{p^2 + M_i^2}}p^2 dp, \tag{25}$$

where the Fermi momentum of the ith quark flavor p_F^i is related to the corresponding quark density ρ_i via

$$\rho_i = \frac{\left(p_F^i\right)^3}{\pi^2}. \tag{26}$$

For a neutral mixture of quarks and leptons, the β-equilibrium conditions are specified by

$$\mu_{s^-} = \mu_{d^-} = \mu_{u^+} + \mu_{e^-}, \quad \mu_{\mu^-} = \mu_{e^-}. \tag{27}$$

In addition, the charge neutrality condition can be written as

$$2y_{u^+} - (y_{d^-} + y_{s^-}) - (y_{e^-} + y_{\mu^-}) = 0, \tag{28}$$

where $y_{(i=u,d,s)} = \frac{\rho_i}{3\rho_B}$ is introduced as the relative fraction of the ith quark for a given baryonic density $\rho_B = (\rho_u + \rho_d + \rho_s)/3$. Here ρ_B is employed as an input for solving the coupled equations self-consistently. Thus, the energy density and pressure of quark matter in β equilibrium are given by

$$e_Q = e_{\rm NJL} + e_L, \tag{29}$$

$$P_Q = P_{\rm NJL} + P_L = \sum_{k=u,d,s,e,\mu} n_k\mu_k - e_Q, \tag{30}$$

where

$$\begin{aligned} e_{\rm NJL} &= \sum_{i=u,d,s}\left[-\frac{3}{\pi^2}\int_{p_F^i}^{\Lambda}\sqrt{p^2 + (M_i)^2}p^2 dp\right] \\ &\quad +2G_S\left(C_u^2 + C_d^2 + C_s^2\right) - 4KC_uC_dC_s - e_{\rm NJL}^{(0)}. \end{aligned} \tag{31}$$

In the above relation, $e_{\rm NJL}^{(0)}$ is included to ensure the requirement $e_{\rm NJL} = 0$ in the vacuum.

Finally, it is necessary to mention that the vector interaction shifts the quark chemical potential μ_i and energy density $e_{\rm NJL}$ as follows [39]:

$$\mu_i \to \mu_i - 4G_V\rho_i \Longrightarrow \mu_i = \sqrt{(p_F^i)^2 + (M_i)^2} + 4G_V\rho_i, \tag{32}$$

and

$$e_{\rm NJL} \to e_{\rm NJL} - 2G_V\sum_{i=u,d,s}\rho_i^2. \tag{33}$$

Therefore, $e_{\rm NJL}$ in the presence of the vector interaction is obtained by including the repulsive term $+2G_V\sum_{i=u,d,s}\rho_i^2$ in the expression of Eq. (31).

C. Maxwell and Gibbs constructions

The Maxwell and Gibbs constructions are generally adopted as the well-known approaches for studying the baryon-quark phase transition. For the Maxwell construction, a sharp phase transition between baryonic and quark matter is formed, which leads to the disappearance of the mixed phase region. As a local constraint, pure phases in the Maxwell construction are independently charge neutral. Furthermore, the phase transition conditions for the Maxwell construction are given by

$$\mu_n\left[\rho_B^{(BP)}\right] = 2\mu_d\left[\rho_B^{(QP)}\right] + \mu_u\left[\rho_B^{(QP)}\right] \equiv \mu_n\left[\rho_B^{(QP)}\right], \tag{34}$$

$$P\left[\rho_B^{(BP)}\right] = P\left[\rho_B^{(QP)}\right]. \tag{35}$$

The energy density of the mixed phase at the constant P and μ_n is obtained by

$$e = \rho_B\mu_n - P. \tag{36}$$

For the Gibbs construction, the pressure of the mixed phase is not constant. The requirement of charge neutrality is imposed globally for the Gibbs construction. In addition, for a given pressure P, the following conditions hold between baryonic and quark matter in the mixed phase:

$$\mu_n^{(BP)} = \mu_n^{(QP)} \equiv \mu_n, \tag{37}$$

$$\mu_e^{(BP)} = \mu_e^{(QP)} \equiv \mu_e, \tag{38}$$

$$P = P^{(BP)}[\mu_n, \mu_e] = P^{(QP)}[\mu_n, \mu_e]. \tag{39}$$

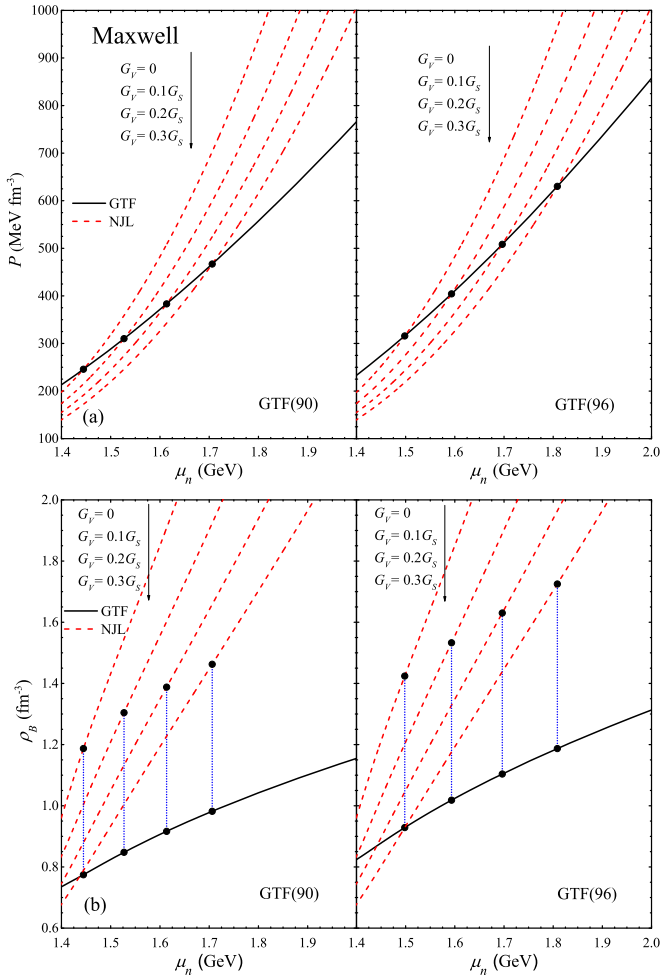

FIG. 1. (a) Pressure and (b) baryon density as functions of the neutron chemical potential for the GTF(90) and GTF(96) interactions (solid lines), and the NJL model at $G_V = 0, 0.1G_S,\ 0.2G_S,\ 0.3G_S$ (dashed lines). The vertical dotted lines show the ranges of the baryon-quark mixed phase, according to the Maxwell construction.

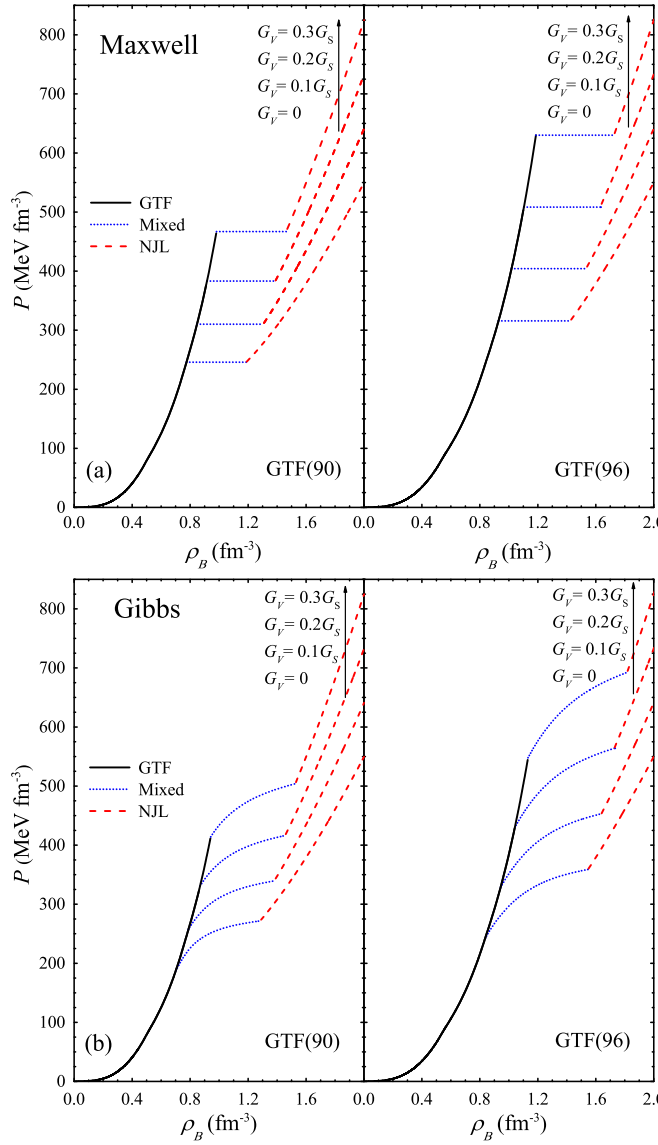

FIG. 2. Pressure as a function of baryon density for the GTF(90) and GTF(96) interactions (solid lines), and the NJL model at $G_V = 0, 0.1G_S,\ 0.2G_S,\ 0.3G_S$ (dashed lines), according to the (a) Maxwell and (b) Gibbs constructions. The dotted lines show the ranges of the baryon-quark mixed phase.

Consequently, the volume fraction χ $(0 \leqslant \chi \leqslant 1)$ occupied by baryonic matter in the mixed phase is obtained from the condition of global charge neutrality as follows:

$$\chi \rho_C^{(BP)} + (1-\chi)\rho_C^{(QP)} = 0, \tag{40}$$

where

$$\rho_C^{(BP)} = \rho_{p^+}^{(BP)} + \rho_{\Sigma^+}^{(BP)} - \rho_{\Sigma^-}^{(BP)} - \rho_{\Xi^-}^{(BP)} - \rho_{e^-}^{(BP)} - \rho_{\mu^-}^{(BP)}, \tag{41}$$

$$\rho_C^{(QP)} = \frac{2}{3}\rho_{u^+}^{(QP)} - \frac{1}{3}\rho_{d^-}^{(QP)} - \frac{1}{3}\rho_{s^-}^{(QP)} - \rho_{e^-}^{(QP)} - \rho_{\mu^-}^{(QP)}. \tag{42}$$

Consequently, the baryonic density ρ_B and energy density e in the mixed phase are extracted from

$$\rho_B = \chi \rho^{(BP)} + (1-\chi)\rho^{(QP)}, \tag{43}$$

$$e = \chi e^{(BP)} + (1-\chi)e^{(QP)}. \tag{44}$$

III. RESULTS AND DISCUSSIONS

In the general trend of this research, using the GTF(90) and GTF(96) interactions for baryonic matter and the NJL model for quark matter, the baryon-quark phase transition is studied for the four values of the vector coupling constant $G_V = 0,\ 0.1G_S,\ 0.2G_S,\ 0.3G_S$, according to the Maxwell and Gibbs constructions.

Figure 1 displays the pressure P and baryonic density ρ_B as a function of the neutron chemical potential μ_n for the TF and NJL models. The intersection between the baryonic and quark EOSs shows the coexistence point, according to the Maxwell construction. Such an intersection is a necessary but not sufficient condition for the Gibbs construction. Corresponding to the intersection points, the baryonic density ranges for the

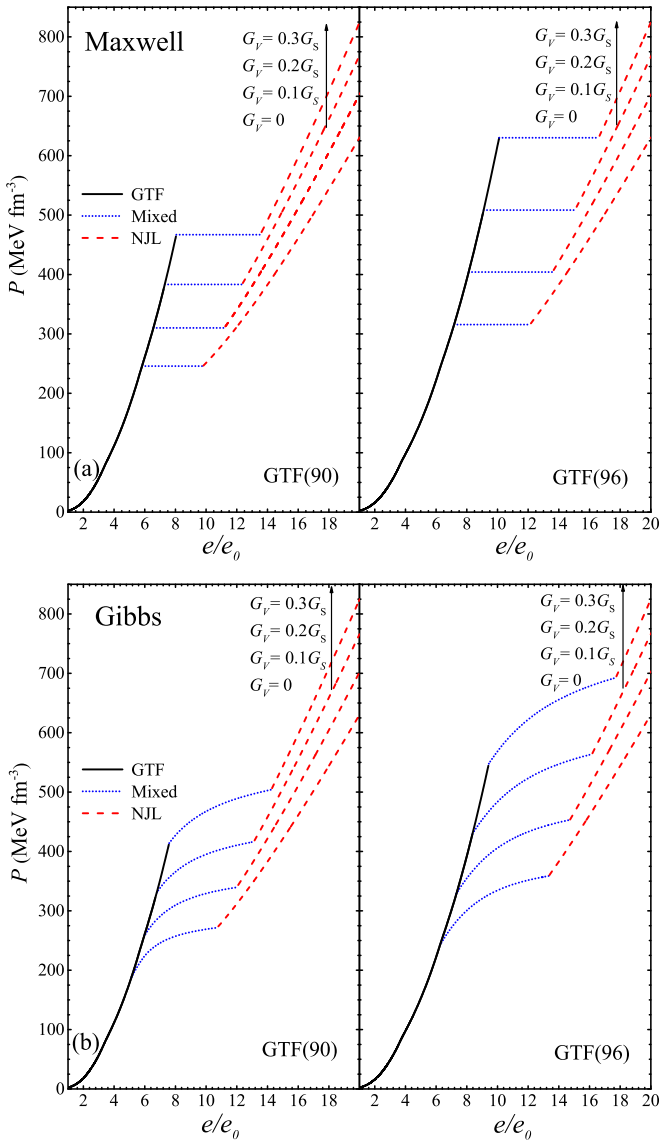

FIG. 3. Pressure as a function of energy density (in units of e_0) for the GTF(90) and GTF(96) interactions (solid lines), and the NJL model at $G_V = 0, 0.1G_S,\ 0.2G_S,\ 0.3G_S$ (dashed lines), according to the (a) Maxwell and (b) Gibbs constructions. The dotted lines show the ranges of the baryon-quark mixed phase.

baryon-quark coexistence are shown in the lower panels of this figure. As G_V is changed from 0 to $0.3G_S$, the increase of P with respect to μ_n becomes slower in the quark EOS. Therefore, the intersection points are pushed to the higher values.

Since the pressure is one of the most remarkable aspects of the EOS for NS matter, the baryonic density and energy density dependences are displayed in Figs. 2 and 3, respectively. As shown in these figures, the stiffness of the EOS depends seriously on the nature of the interactions used for baryonic and quark matter. Such a stiffness has a significant effect on the threshold formation of the mixed phase of baryons and quarks. Thus, since the GTF(90) interaction is more repulsive, the baryonic EOS is stiffer than the one for the GTF(96) interaction. It is seen that with increasing G_V, the quark EOS shows a stiffer behavior. Moreover, the width of the mixed phase region is reduced by a stiffer baryonic EOS, while it is slightly increased by a stiffer quark EOS. Furthermore, in contrast to a stiffer baryonic EOS, a stiffer quark EOS shifts the onset of the phase transition to the higher baryonic or energy densities. Unlike the Maxwell construction, the pressure of the mixed phase in the Gibbs construction is not constant and, therefore, is a slow increasing function of baryonic or energy density. In Table II, the baryonic and energy density widths of the mixed phases are listed for both Maxwell and Gibbs constructions. It is clear that the region of the mixed phase for the Maxwell construction is located inside that for the Gibbs construction. In addition, the widths of the mixed phase in the Maxwell and Gibbs constructions become closer to each other, as G_V varies from 0 to $0.3G_S$.

The stability of the baryon-quark mixed phase under the Maxwell and Gibbs constructions can be studied by the Debye screening length and the amount of Coulomb and surface energy needed for the formation of baryonic and quark structures [52,53]. Hence, the total Coulomb and surface energy density $e_{\rm Coul} + e_{\rm surf}$ can be written in the context of the approach for studying the nuclear pasta in the inner crust of NSs [54–56]:

$$\Delta e_\sigma = e_{\rm Coul} + e_{\rm surf} = 3\eta d\left[\frac{\pi\sigma_s^2 q_e^2\left(\rho_C^{(BP)} - \rho_C^{(QP)}\right)^2\varphi_d(\eta)}{2d}\right]^{\frac{1}{3}}, \tag{45}$$

where η, d, σ_s, q_e are the volume fraction occupied by the less abundant phase (i.e., $\eta = \chi$ for $\chi > 0.5$ and $\eta = 1 - \chi$ for $\chi \leqslant 0.5$), geometrical dimension of Wigner-Seitz cells ($d = 1, 2$, and 3 correspond to the case of slabs, rods, and spheres, respectively), surface tension between baryonic and quark matter, magnitude of the electron charge, and

$$\varphi_d(\eta) = \frac{1}{d+2}\left[\eta + \frac{2 - d\eta^{1-(2/d)}}{d-2}\right]. \tag{46}$$

The mixed phase is energetically favorable if $\Delta e_\sigma = e(\sigma_s) - e(\sigma_s = 0)$ is less than $\Delta e_M = e_M - e(\sigma_s = 0)$ [e_M and $e(\sigma_s = 0)$ are the energy density obtained from Eqs. (36) and (44) for the Maxwell and Gibbs constructions, respectively]. Since the value of σ_s at the interface between baryonic and quark matter is not known, Δe_σ from Eq. (45) can be calculated for a range of σ_s, by carrying out a numerical minimization with respect to the value of d. Within this formalism, the results of our calculations for the mixed phase, extracted from the GTF(90) and GTF(96) interactions, are presented in Figs. 4 and 5, respectively. The solid and dashed lines show Δe_σ at different values of σ_s and Δe_M as a function of baryonic density in the mixed phase, respectively. As indicated, the mixed phase is always energetically favorable for $\sigma_s \sim 2$ MeV fm^{-2}, while by using the GTF(90) [GTF(96)] interaction, for σ_s in the range $\approx$2–5 (2–10) MeV fm^{-2}, the mixed phase is energetically favorable over a baryonic density region larger than the mixed region in the Maxwell construction. In addition, for $\sigma_s \gtrsim 60$ (80) MeV fm^{-2}, the Maxwell construction becomes always energetically favorable in GTF(90) [GTF(96)]. While enforcing the repulsive vector interaction in the quark phase,

TABLE II. Widths of mixed phases in terms of baryonic density, and energy density (in units of e_0) for the GTF(90) and GTF(96) interactions, joined with the NJL model at $G_V = 0, 0.1G_S, 0.2G_S, 0.3G_S$ under the Maxwell and Gibbs constructions.

	GTF(90)		GTF(96)	
	$\rho^{(BP)} - \rho^{(QP)}$ (fm^{-3})	$e^{(BP)} - e^{(QP)}$ (e_0)	$\rho^{(BP)} - \rho^{(QP)}$ (fm^{-3})	$e^{(BP)} - e^{(QP)}$ (e_0)
Maxwell:				
$G_V = 0$	$0.77 - 1.19$	$5.82 - 9.79$	$0.93 - 1.42$	$7.17 - 12.12$
$G_V = 0.1G_S$	$0.85 - 1.30$	$6.56 - 11.21$	$1.02 - 1.53$	$8.12 - 13.59$
$G_V = 0.2G_S$	$0.92 - 1.39$	$7.30 - 12.37$	$1.10 - 1.63$	$9.10 - 15.05$
$G_V = 0.3G_S$	$0.98 - 1.46$	$8.06 - 13.52$	$1.19 - 1.73$	$10.11 - 16.60$
Gibbs:				
$G_V = 0$	$0.70 - 1.28$	$5.13 - 10.72$	$0.84 - 1.55$	$6.27 - 13.35$
$G_V = 0.1G_S$	$0.79 - 1.38$	$5.95 - 11.99$	$0.94 - 1.64$	$7.32 - 14.72$
$G_V = 0.2G_S$	$0.87 - 1.46$	$6.78 - 13.11$	$1.04 - 1.73$	$8.37 - 16.16$
$G_V = 0.3G_S$	$0.94 - 1.53$	$7.59 - 14.24$	$1.13 - 1.82$	$9.44 - 17.71$

the Maxwell construction becomes energetically favorable at higher values of σ_s.

Determining the EOS of NS matter in a broad range of baryonic density helps us extract the relation between pressure and energy density, $P = P(e)$, as an input in the well-known Tolman-Oppenheimer-Volkoff (TOV) equations for computing the mass of NSs in terms of their radius and central energy density [57]:

$$\frac{dP(r)}{dr} = -\frac{Gm(r)e(r)}{r^2}\frac{\left[1+\frac{P(r)}{e(r)c^2}\right]\left[1+\frac{4\pi r^3 P(r)}{m(r)c^2}\right]}{1-\frac{2Gm(r)}{rc^2}}, \quad (47)$$

$$\frac{dm(r)}{dr} = 4\pi r^2 e(r), \quad (48)$$

where G, P, e, and m are the gravitational constant, pressure, energy density, and mass enclosed within a radius r, respectively. Thus, by solving the TOV equations, the equilibrium configuration of NSs is obtained. The calculations start from a central energy density e_c up to the energy density of iron in the surface. At the medium baryonic density $0.001 \leqslant \rho_B \leqslant 0.08$ fm^{-3}, the EOS of Negele and Vauthrun [58], which is based on the Hartree-Fock approach, is used for the inner crust of NSs. For the outer crust of NSs, the EOS of Baym *et al.* [59], which relies on the properties of heavy nuclei, is employed in the low baryonic density regime $\rho_B < 0.001$ fm^{-3}. For all cases of NS matter, the output values of the gravitational mass as a function of the central energy density e_c (in units of e_0) and total radius R are shown in Figs. 6 and 7, respectively. It is clearly seen from these figures that the gravitational mass reaches a maximum value, as reported in Table III for each case of NS matter. On the other hand, the maximum mass must be consistent with the PSR J0348 + 0432 (PSR J1614 − 2230) mass measurement of $2.01M_\odot \pm 0.04M_\odot$ [42] ($1.928M_\odot \pm 0.017M_\odot$ [41]), as an indication that the EOS of NS matter is valid. As expected from the behavior of the baryonic EOS, the obtained maximum masses in the GTF(90) interaction are greater than the ones in the GTF(96) interaction. Furthermore, the vector

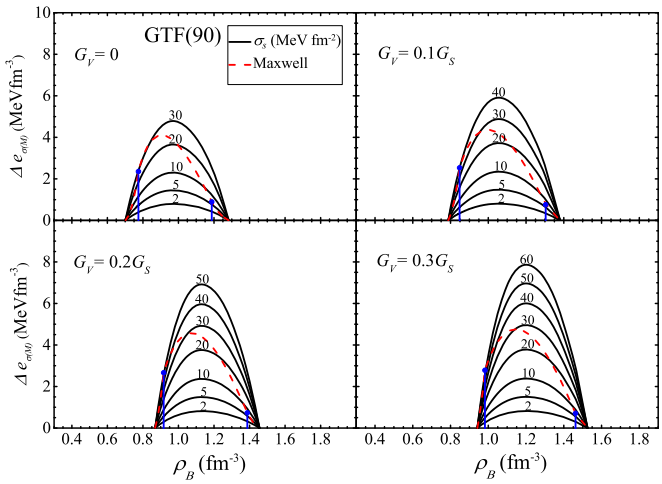

FIG. 4. The solid lines show the baryonic density dependence of Δe_σ at different values of σ_s. The dashed lines correspond to Δe_M and the vertical lines mark the limits of the mixed region for the Maxwell construction. The mixed phase are described by the GTF(90) interaction for baryonic matter and the NJL model for quark matter at $G_V = 0, 0.1G_S,\ 0.2G_S,\ 0.3G_S$.

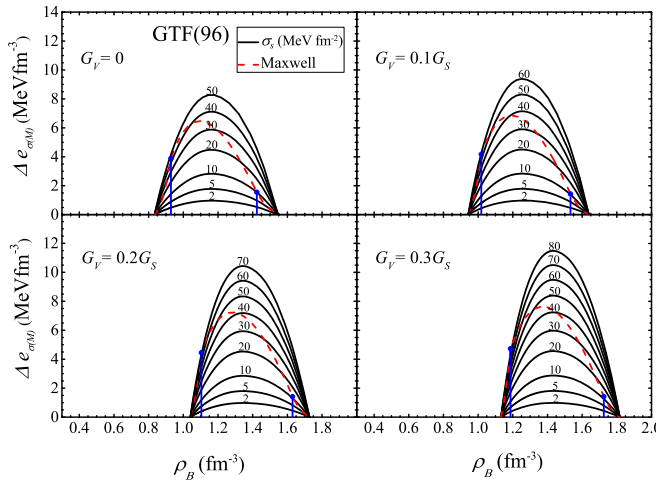

FIG. 5. Same as Fig. 4 but for the GTF(96) interaction.

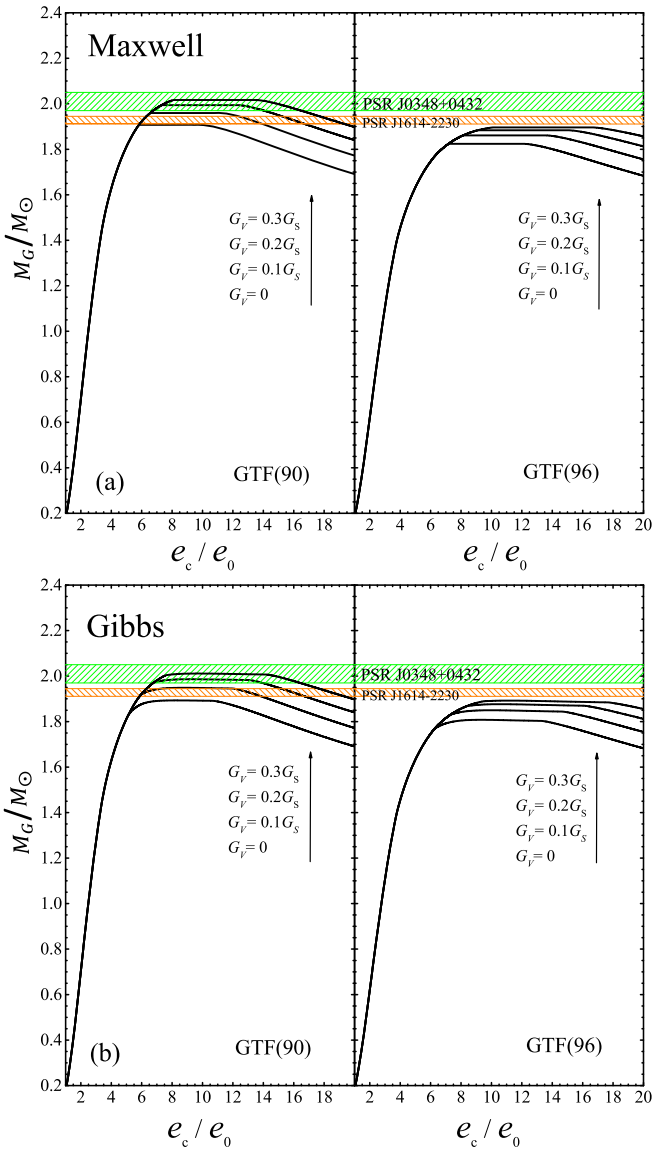

FIG. 6. The gravitational mass of NSs (in units of $M_\odot$) as a function of the central energy density (in units of e_0) for the GTF(90) and GTF(96) interactions, joined with the NJL model at $G_V = 0, 0.1G_S,\ 0.2G_S,\ 0.3G_S$ under the (a) Maxwell and (b) Gibbs constructions. The upper (lower) horizontal band shows the observational constraint from PSR J0348 + 0432 (PSR J1614 − 2230) mass measurement of $2.01M_\odot \pm 0.04M_\odot$ [42] ($1.928M_\odot \pm 0.017M_\odot$ [41]).

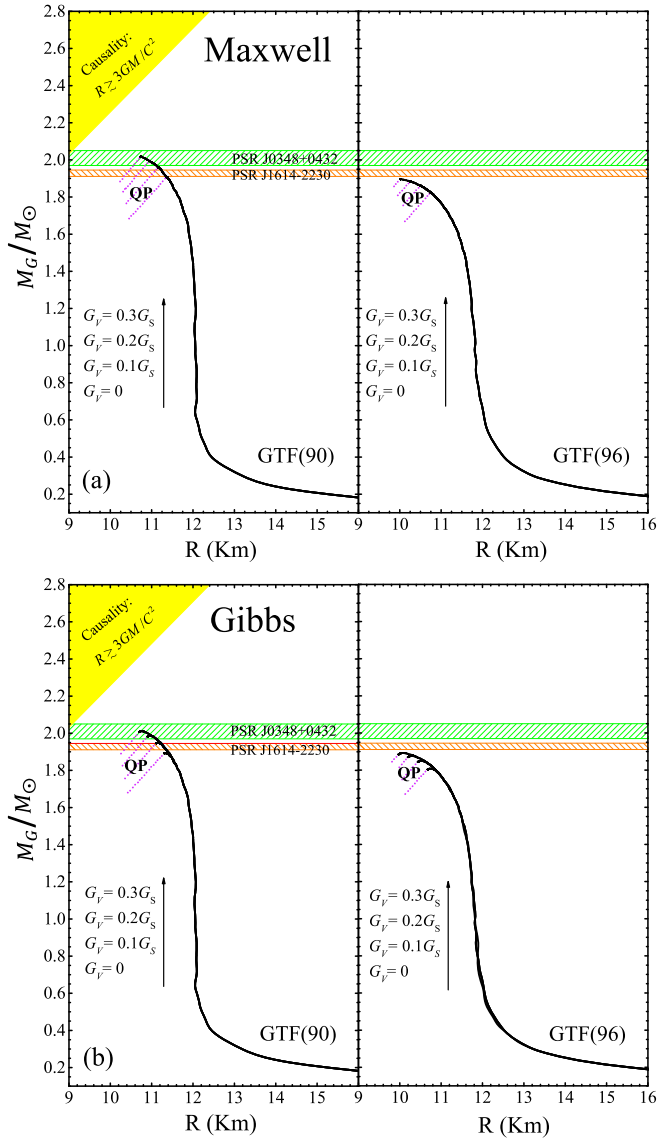

FIG. 7. Mass-radius diagrams for the GTF(90) and GTF(96) interactions, joined with the NJL model at $G_V = 0, 0.1G_S,\ 0.2G_S,\ 0.3G_S$ under the (a) Maxwell and (b) Gibbs constructions. The dotted lines indicate the pure quark phase in the inner core of NSs. The upper (lower) horizontal band shows the observational constraint from PSR J0348 + 0432 (PSR J1614 − 2230) mass measurement of $2.01M_\odot \pm 0.04\ M_\odot$ [42] ($1.928M_\odot \pm 0.017\ M_\odot$ [41]). The regions on the top-left of each panel are excluded by causality [2].

interaction in the NJL model has a significant influence on the maximum mass of NSs. An important outcome of the vector interaction is the possibility of forming quark degrees of freedom in the inner core of NSs, since the maximum masses increase effectively with G_V. As seen in Table III, the maximum masses of NSs for the different EOSs are in the range $1.824M_\odot$–$2.017M_\odot$ ($1.808M_\odot$–$2.011M_\odot$) under the Maxwell (Gibbs) construction. The maximum masses for the Maxwell construction are slightly larger than those for the Gibbs construction, but both of them become closer to each other with rising G_V. It can be understood from Fig. 7 that the presence of a pure quark phase in the inner core indicates an unstable hybrid NS against radial oscillations, because the corresponding gravitational mass lies to the left of the respective mass peak in the mass-radius diagram [38]. Hence, our results show that a stable hybrid NS cannot be formed under the Maxwell construction, since the existence of a pure quark phase in the inner core is ruled out [37].

According to the Gibbs construction, the composition of NS matter can be investigated by considering the baryon-quark mixed phase. The relative fraction of particles y_i as a function of the baryonic density ρ_B are displayed in Figs. 8

TABLE III. Maximum masses of NSs (in units of $M_\odot$) for the GTF(90) and GTF(96) interactions, joined with the NJL model at $G_V = 0, 0.1G_S, 0.2G_S, 0.3G_S$ under the Maxwell and Gibbs constructions. e_c and P_c are the corresponding central energy density (in units of e_0) and pressure, respectively. R is the total radius of NSs.

	GTF(90)				GTF(96)			
	e_c (e_0)	P_c $\left(10^{35}\frac{\text{dyn}}{\text{cm}^2}\right)$	$M_{\max}$ ($M_\odot$)	R (km)	e_c (e_0)	P_c $\left(10^{35}\frac{\text{dyn}}{\text{cm}^2}\right)$	$M_{\max}$ ($M_\odot$)	R (km)
Maxwell:								
$G_V = 0$	5.82 – 9.79	3.95	1.908	11.36	7.17 – 12.12	5.08	1.824	10.75
$G_V = 0.1G_S$	6.56 – 11.21	4.99	1.960	11.16	8.12 – 13.59	6.50	1.861	10.50
$G_V = 0.2G_S$	7.30 – 12.37	6.16	1.994	10.27	9.10 – 15.05	8.18	1.884	10.27
$G_V = 0.3G_S$	8.06 – 13.52	7.51	2.017	10.74	10.11 – 16.60	10.13	1.896	10.01
Gibbs:								
$G_V = 0$	8.30	4.18	1.893	11.33	9.30	5.23	1.808	10.73
$G_V = 0.1G_S$	8.80	5.14	1.949	11.15	10.00	6.53	1.850	10.53
$G_V = 0.2G_S$	9.30	6.23	1.986	10.95	10.60	8.01	1.877	10.30
$G_V = 0.3G_S$	9.80	7.47	2.011	10.77	11.20	9.71	1.892	10.09

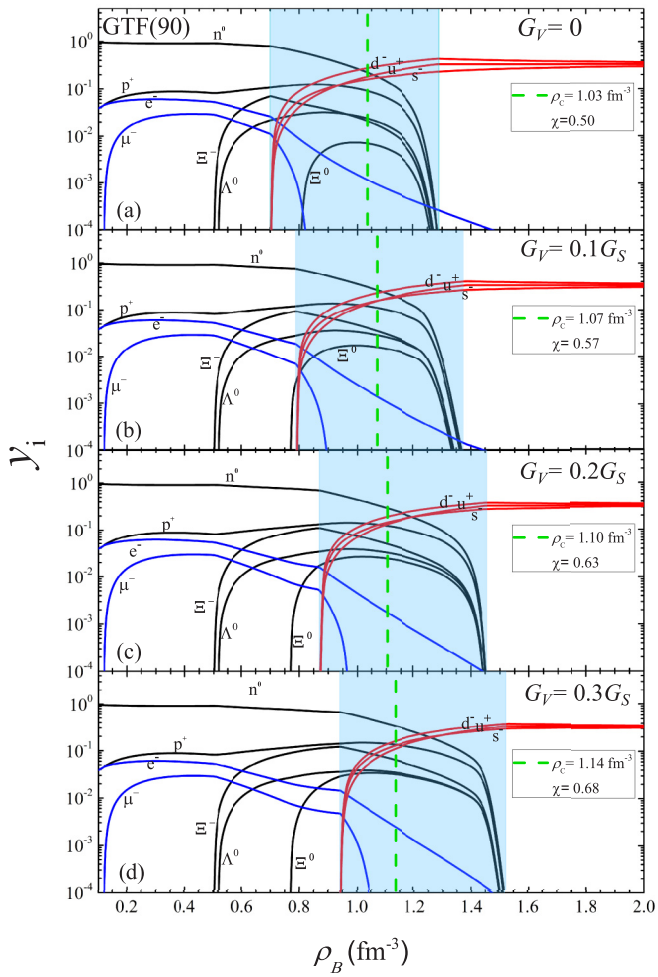

FIG. 8. Relative fractions of baryons, leptons, and quarks for the GTF(90) interaction, joined with the NJL model at (a) $G_V = 0$, (b) $G_V = 0.1G_S$, (c) $G_V = 0.2G_S$, and (d) $G_V = 0.3G_S$. The areas of the mixed phase are highlighted. The dashed vertical lines show the central baryonic density of NSs ρ_c with the baryonic volume fraction χ, corresponding to the maximum gravitational masses under the Gibbs construction.

and 9 for GTF(90) and GTF(96), respectively. As predicted by various theoretical models, the neutrons have the most abundance among the baryons. It is seen that at the lower baryonic densities, the proton, electron, and muon fractions increase rapidly with baryonic density, while the neutron

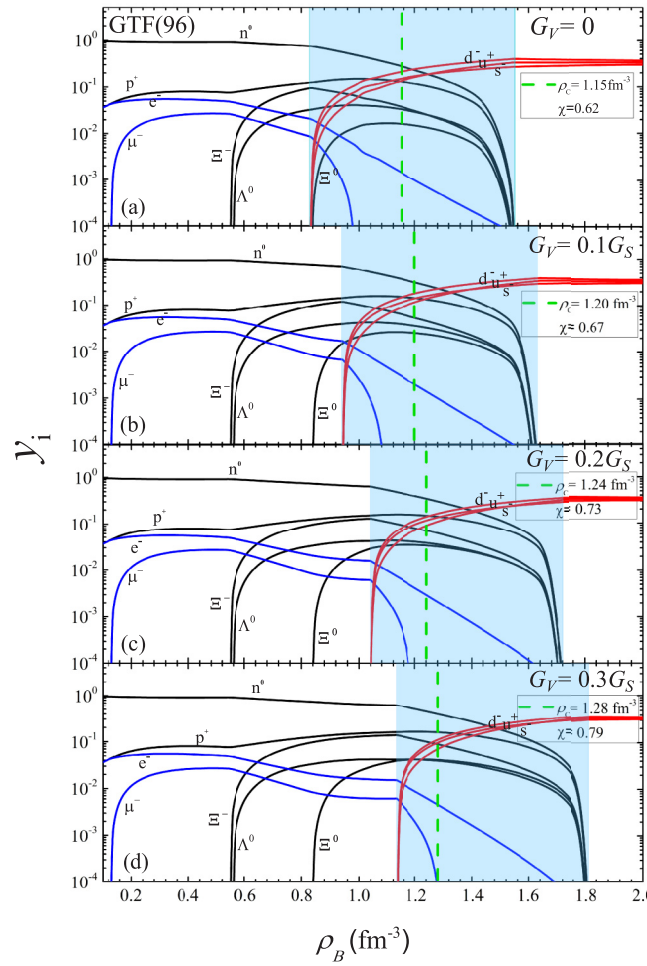

FIG. 9. Same as Fig. 8 but for the GTF(96) interaction.

TABLE IV. Width of mixed phase in terms of baryonic density, and central baryonic density ρ_c together with baryonic volume fraction χ (corresponding to the maximum mass of NSs in units of $M_\odot$) for the GTF(90) and GTF(96) interactions, joined with the NJL model at the canonical Fierz value $G_V = 0.5G_S$ under the Gibbs construction. R is the total radius of NSs.

	$\rho^{(BP)} - \rho^{(QP)}$ (fm^{-3})	ρ_c (fm^{-3})	χ	$M_{\max}$ ($M_\odot$)	R (km)
GTF(90):	1.08 − 1.66	1.18	0.83	2.035	10.39
GTF(96):	1.31 − 2.00	1.29	1	1.901	9.73

fraction is a slow decreasing function of baryonic density. The existence of hyperons has a substantial impact on the EOS of NS matter at the higher baryonic densities. Hyperons can constitute a considerable baryonic portion of NS matter. The formation of hyperons is delayed up to densities of about $3.2\rho_0$, once the Ξ^- hyperon appears. The appearance of the Ξ^- hyperon accelerates the deleptonization of NS matter, due to the charge neutrality condition. The consequence of more repulsive effects in GTF(90) is the earlier appearance of hyperons in the baryonic density range than in GTF(96). In the pure quark phase, the relation $y_s < y_u < y_d$ holds. In addition, the relative fractions of u, d, and s quarks reach the plateaus with rising baryonic density. At extremely high baryonic densities, the relation $y_s \sim y_u \sim y_d \sim 1/3$ is established, due to the restoration of chiral symmetry. The areas of the baryon-quark mixed phase are also denoted in these figures. When the baryon-quark phase transition occurs, the relative fractions of quarks increase rapidly with the baryonic density. The higher values of G_V suppress the threshold formation of the mixed phase to the higher baryonic densities. On the other hand, the width of the mixed phase is slightly extended with increment of G_V. For the sake of clarity, the central baryonic density ρ_c together with the baryonic volume fraction χ, corresponding to the maximum gravitational mass of NSs, are presented in these figures.

It is instructive to compare these findings with those calculated from the canonical Fierz value $G_V = 0.5G_S$ (see Table IV). Consequently, as G_V is increased, ρ_c is pushed toward higher values, while unlike those presented in Ref. [39] for the hadronic model parametrization GM1 in the standard (local) NJL model, the region of the mixed phase shrinks in the inner core of NSs.

IV. SUMMARY AND CONCLUSION

In this paper, we have investigated the EOS of NS matter including the baryon-quark phase transition. Such an EOS has a clear connection with our understanding about the structure of hybrid NSs. The TF approximation has been employed in a semiclassical MF model to describe the baryonic EOS by the GTF(90) and GTF(96) interactions. The results reflect the stiffer nature of the baryonic EOS in GTF(90) because of being more repulsive than GTF(96). For the EOS of quark matter, we have considered the NJL model. The deconfinement phase transition in NS matter has been studied under the Maxwell and Gibbs constructions. We have shown that the repulsive vector interaction, specified by the vector coupling constant G_V in the NJL model, has a small (significant) effect on the width (threshold formation) of the baryon-quark mixed phase. In addition, with increasing G_V, the Maxwell construction becomes energetically favorable at higher values of the surface tension between baryonic and quark matter. Within the present research, the inner core of NSs can be formed with a region of the baryon-quark mixed phase, but the formation of a pure quark phase is excluded. Hence, the Maxwell construction provides an unstable hybrid star for both the GTF(90) and GTF(96) interactions. When the value of G_V is increased, the mixed phase region of the inner core shrinks, since the quark EOS becomes stiffer. Evidently, the stiffer EOSs reach the higher values of the maximum mass. In addition, the maximum masses in the Maxwell construction are slightly larger than those in the Gibbs construction. This approach can be extended to the finite temperatures to investigate the baryon-quark phase transition in the interior of protoneutron stars.

ACKNOWLEDGMENT

The authors thank the University of Kashan for supporting this project under Grant No. 785227/3 provided by the Research Council.

[1] H. A. Bethe, Rev. Mod. Phys. **62**, 801 (1990).
[2] J. M. Lattimer and M. Prakash, Science **304**, 536 (2004).
[3] M. Camenzind, *Compact Objects in Astrophysics* (Springer-Verlag, Berlin, 2007).
[4] S. L. Shapiro and S. A. Teukolsky, *Black Holes, White Dwarfs and Neutron Stars* (Wiley, New York, 2008).
[5] F. Weber, *Pulsars as Astrophysical Laboratories for Nuclear and Particle Physics*, High Energy Physics, Cosmology and Gravitation Series (IOP Publishing, Bristol, Great Britain, 1999).
[6] N. K. Glendenning, *Compact Stars, Nuclear Physics, Particle Physics, and General Relativity*, 2nd ed. (Springer-Verlag, New York, 2000).
[7] P. Haensel, A. Y. Potekhin, and D. G. Yakovlev, *Neutron Stars 1: Equation of State and Structure*, Vol. 326 (Springer Science and Business Media, New York, 2007).
[8] M. Baldo, G. F. Burgio, and H. J. Schulze, Phys. Rev. C **61**, 055801 (2000).
[9] I. Vidaña, A. Polls, A. Ramos, L. Engvik, and M. Hjorth-Jensen, Phys. Rev. C **62**, 035801 (2000).
[10] H. J. Schulze and T. Rijken, Phys. Rev. C **84**, 035801 (2011).
[11] I. Vidaña, D. Logoteta, C. Providência, A. Polls, and I. Bombaci, Europhys. Lett. **94**, 11002 (2011).
[12] H. Đapo, B.-J. Schaefer, and J. Wambach, Phys. Rev. C **81**, 035803 (2010).
[13] S. Weissenborn, D. Chatterjee, and J. Schaffner-Bielich, Phys. Rev. C **85**, 065802 (2012).

[14] H. R. Moshfegh and M. Ghazanfari Mojarrad, Eur. Phys. J. A **49**, 1 (2013).
[15] M. Ghazanfari Mojarrad and R. Arabsaeidi, Int. J. Mod. Phys. E **25**, 1650102 (2016).
[16] W. D. Myers, Ann. Phys. (NY) **204**, 401 (1990).
[17] W. D. Myers and W. J. Swiatecki, Nucl. Phys. A **601**, 141 (1996).
[18] J. Randrup and E. Lima Medeiros, Nucl. Phys. A **529**, 115 (1991).
[19] K. Strobel, F. Weber, and M. K. Weigel, Z. Naturforsch. A **54**, 83 (1999).
[20] H. R. Moshfegh and M. Ghazanfari Mojarrad, J. Phys. G **38**, 085102 (2011).
[21] M. Ghazanfari Mojarrad and S. K. Mousavi Khoroshtomi, Int. J. Mod. Phys. E **26**, 1750038 (2017).
[22] M. Ghazanfari Mojarrad, N. S. Razavi, and S. Vaezzade, Nucl. Phys. A **980**, 51 (2018).
[23] M. Ghazanfari Mojarrad and N. S. Razavi, Nucl. Phys. A **986**, 133 (2019).
[24] N. K. Glendenning, Phys. Rev. D **46**, 1274 (1992).
[25] M. G. Alford, K. Rajagopal, S. Reddy, and F. Wilczek, Phys. Rev. D **64**, 074017 (2001).
[26] M. G. Alford, A. Schmitt, K. Rajagopal, and T. Schäfer, Rev. Mod. Phys. **80**, 1455 (2008).
[27] C. Maieron, M. Baldo, G. F. Burgio, and H. J. Schulze, Phys. Rev. D **70**, 043010 (2004).
[28] F. Weber, Prog. Part. Nucl. Phys. **54**, 193 (2005).
[29] D. B. Blaschke, D. Gomez Dumm, A. G. Grunfeld, T. Klähn, and N. N. Scoccola, Phys. Rev. C **75**, 065804 (2007).
[30] T. Klähn *et al.*, Phys. Lett. B **654**, 170 (2007).
[31] T. Klähn and T. Fischer, Astrophys. J. **810**, 134 (2015).
[32] A. Sedrakian, Prog. Part. Nucl. Phys. **58**, 168 (2007).
[33] F. Yang and H. Shen, Phys. Rev. C **77**, 025801 (2008).
[34] O. Benhar and A. Cipollone, Astron. Astrophys. **525**, L1 (2011).
[35] H. Chen, M. Baldo, G. F. Burgio, and H. J. Schulze, Phys. Rev. D **84**, 105023 (2011).
[36] L. Bonanno and A. Sedrakian, Astron. Astrophys. **539**, A16 (2012).
[37] D. Logoteta, C. Providência, and I. Vidaña, Phys. Rev. C **88**, 055802 (2013).
[38] M. Orsaria, H. Rodrigues, F. Weber, and G. A. Contrera, Phys. Rev. D **87**, 023001 (2013).
[39] M. Orsaria, H. Rodrigues, F. Weber, and G. A. Contrera, Phys. Rev. C **89**, 015806 (2014).
[40] P. Demorest, T. Pennucci, S. Ransom, M. Roberts, and J. Hessels, Nature **467**, 1081 (2010).
[41] E. Fonseca *et al.*, Astrophys. J. **832**, 167 (2016).
[42] J. Antoniadis *et al.*, Science **340**, 1233232 (2013); R. S. Lynch *et al.*, Astrophys. J. **763**, 81 (2013).
[43] Y. Nambu and G. Jona-Lasinio, Phys. Rev. **122**, 345 (1961). **124**, 246 (1961).
[44] M. Buballa, Phys. Rep. **407**, 205 (2005).
[45] M. Brack and R. K. Bhaduri, *Semiclassical Physics* (Addison-Wesley, Boston, 1997); M. Brack, C. Guet, and H. B. Hakansson, Phys. Rep. **123**, 275 (1985).
[46] J. Schaffner, C. Greiner, and H. Stöcker, Phys. Rev. C **46**, 322 (1992).
[47] E. Friedman and A. Gal, Phys. Rep. **452**, 89 (2007).
[48] I. Bednarek, P. Haensel, J. L. Zdunik, M. Bejger, and R. Mańka, Astron. Astrophys. **543**, A157 (2012).
[49] P. Rehberg, S. P. Klevansky, and J. Hüfner, Phys. Rev. C **53**, 410 (1996).
[50] C. Sasaki, B. Friman, and K. Redlich, Phys. Rev. D **75**, 054026 (2007).
[51] Z. Zhang and T. Kunihiro, Phys. Rev. D **80**, 014015 (2009).
[52] H. Heiselberg, C. J. Pethick, and E. F. Staubo, Phys. Rev. Lett. **70**, 1355 (1993).
[53] H. Heiselberg and V. R. Pandharipande, Annu. Rev. Nucl. Part. Sci. **50**, 481 (2000).
[54] D. G. Ravenhall, C. J. Pethick, and J. R. Wilson, Phys. Rev. Lett. **50**, 2066 (1983).
[55] T. Maruyama, T. Tatsumi, D. N. Voskresensky, T. Tanigawa, and S. Chiba, Phys. Rev. C **72**, 015802 (2005).
[56] O. Benhar and R. Rubino, Astron. Astrophys. **434**, 247 (2005).
[57] R. C. Tolman, Phys. Rev. **55**, 364 (1939); J. R. Oppenheimer and G. M. Volkoff, *ibid.* **55**, 374 (1939).
[58] J. W. Negele and D. Vautherin, Nucl. Phys. A **207**, 298 (1973).
[59] G. Baym, C. Pethick, and D. Sutherland, Astrophys. J. **170**, 299 (1971).